Chinese Journal of Natural Medicines

Jasurolignoside from *Ilex pubescens* exerts a therapeutic effect on acute lung injury *in vitro* and *in vivo* by binding to TLR4

Shan Han, Chi Teng Vong, Jia He, Qinqin Wang, Qiumei Fan, Siyuan Li, Jilang Li, Min Liao, Shilin Yang, Renyikun Yuan, Hongwei Gao

Citation: Shan Han, Chi Teng Vong, Jia He, Qinqin Wang, Qiumei Fan, Siyuan Li, Jilang Li, Min Liao, Shilin Yang, Renyikun Yuan, Hongwei Gao, Jasurolignoside from *Ilex pubescens* exerts a therapeutic effect on acute lung injury *in vitro* and *in vivo* by binding to TLR4, Chinese Journal of Natural Medicines, 2025, 23(9), 1058−1068. doi: 10.1016/S1875−5364(25)60972−1.

View online: https://doi.org/10.1016/S1875−5364(25)60972−1

Chinese Journal of Natural Medicines 23 (2025) 1058-1068

Contents lists available at ScienceDirect

Chinese Journal of Natural Medicines

journal homepage: www.cjnmcpu.com/

Original article

Jasurolignoside from *Ilex pubescens* exerts a therapeutic effect on acute lung injury *in vitro* and *in vivo* by binding to TLR4

Shan Han[a,b], Chi Teng Vong[c], Jia He[a,b], Qinqin Wang[a,b], Qiumei Fan[a], Siyuan Li[a], Jilang Li[a], Min Liao[a], Shilin Yang[a], Renyikun Yuan[a,*], Hongwei Gao[a,*]

[a] *College of Pharmacy, Guangxi University of Chinese Medicine, Nanning, 530200, China*
[b] *National Pharmaceutical Engineering Center for Solid Preparation in Chinese Herbal. Medicine, Jiangxi University of Traditional Chinese Medicine, Nanchang 330006, China*
[c] *State Key Laboratory of Quality Research in Chinese Medicine, Institute of Chinese Medical Sciences, University of Macau, Macau, China*

ARTICLE INFO

Article history:
Received 3 July 2024
Revised 9 October 2024
Accepted 13 October 2024
Available online 20 September 2025

Keywords:
Acute lung injury
Jasurolignoside
TLR4
NF-κB/MAPKs
NLRP3

ABSTRACT

Acute lung injury (ALI) is a severe disease caused by viral infection that triggers an uncontrolled inflammatory response. This study investigated the capacity of jasurolignoside (JO), a natural compound, to bind to Toll-like receptor 4 (TLR4) and treat ALI. The anti-inflammatory properties of JO were evaluated *in vitro* through Western blotting, enzyme-linked immunosorbent assay (ELISA), immunofluorescence staining, and co-immunoprecipitation. The investigation utilized a lipopolysaccharide (LPS)-induced ALI animal model to examine the therapeutic efficacy and mechanism of JO *in vivo*. JO attenuated inflammatory symptoms in infected cells and tissues by modulating the NOD-like receptor family pyrin domain containing protein 3 (NLRP3) inflammasome and the nuclear factor κB (NF-κB)/mitogen-activated protein kinase (MAPK) pathway. Molecular docking simulations revealed JO binding to TLR4 active sites, confirmed by cellular thermal shift assay. Surface plasmon resonance (SPR) demonstrated direct interaction between JO and TLR4 with a Kd value of 35.1 μmol·L^{-1}. Moreover, JO inhibited tumor necrosis factor α (TNF-α), interleukin-1β (IL-1β), and IL-6 secretion and reduced leukocyte, neutrophil, lymphocyte, and macrophage infiltration in ALI-affected mice. JO also enhanced lung function and reduced ALI-related mortality. Immunohistochemical staining demonstrated JO's ability to suppress TLR4 expression in ALI-affected mouse lung tissue. This study establishes that JO can bind to TLR4 and effectively treat ALI, indicating its potential as a therapeutic agent for clinical applications.

1. Introduction

Acute lung injury (ALI) has caused substantial mortality worldwide, leading to respiratory complications including pneumonia and, in severe cases, acute respiratory distress syndrome. ALI represents an aggressive form of viral infection that initiates an uncontrolled inflammatory response [1]. This condition damages alveolar epithelial and lung capillary endothelial cells, resulting in excessive pulmonary inflammation, pulmonary edema, and refractory hypoxemia. Subsequently, critically ill patients may develop respiratory failure [2]. The pathogenesis of ALI is intimately associated with inflammatory cytokine progression, which can substantially exacerbate both pulmonary and systemic inflammatory responses. Various signaling pathways, including nuclear factor κB (NF-κB), mitogen-activated protein kinase (MAPK), nuclear factor erythroid 2-related factor 2 (Nrf2), and NOD-like receptor family pyrin domain containing protein 3 (NLRP3), regulate these inflammatory mediators [3]. The suppression of inflammatory responses induced by the natural immune system may represent a critical approach in ALI treatment.

Toll-like receptor 4 (TLR4), situated in the cell membrane of macrophages and T lymphocytes, recognizes pathogens and activates the innate immune system by forming a complex with CD14, lipopolysaccharide (LPS) binding protein (LBP), and MD2 to establish the TLR4-MD2-LPS complex [4,5]. Subsequently, the TLR4-MD2-LPS complexes form an M-shaped dimer, facilitating the recruitment of the myeloid differentiation primary response 88 (MyD88) protein. This process initiates the activation of the MAPK, Nrf2, and NF-κB pathways, ultimately resulting in the production of pro-inflammatory cytokines [4]. Inflammasomes are multiprotein complexes that assemble in the cytoplasm in response to pathogen infection, serving a vital role in the innate immune system [6]. The NLRP3 inflammasome comprises NLRP3, ASC, and Caspase-1. These components work together to activate pro-Caspase-1, leading to the maturation of pro-cytokines interleukin-1β (IL-1β) and IL-18 [7]. Research has shown that suppressing TLR4 expression alleviates ALI induced by LPS, Pseudomonas aeruginosa secreting type III bacterial, or H9N2 swine influenza virus [8]. Furthermore, activated NLRP3 inflammasome, which facilitates Caspase1 activation, pro-inflammatory cytokine IL-1β/IL-18 secretion, and subsequent accumulation of neutrophils, lymphocytes, and leukocytes in lung tissue, represents a critical factor in ALI development [9, 10]. Therefore, inhibiting TLR4 dimerization and NLRP3 inflammasome activation may present an alternative therapeutic strategy for ALI management.

Jasurolignoside (JO) (Fig. 1A), a neolignan-secoiridoid glucoside, was isolated from *Ilex pubescens* Hook. et Arn. var. *kwangsi-*

* Corresponding author.
E-mail addresses: yryk0808@163.com (R. Yuan); gaohongwei06@126.com (H. Gao)

https://doi.org/10.1016/S1875-5364(25)60972-1

ensis Hand. Mazz [11]. In traditional Chinese medicine, *I. pubescens* has demonstrated therapeutic efficacy in treating cardiovascular diseases, inflammation, and fever [12, 13]. The JO molecule contains an ester bond linking the lignans to the secoiridoid glucoside. The conjugation in iridoids typically occurs at C-7, which undergoes oxidation to form a carboxylic acid before esterification with various moieties [14]. Iridoids conjugated at C-7 exhibit diverse pharmacological activities, including anti-diabetic, anti-inflammatory, immune-suppressive, and anti-tumor effects [15]. This study investigated the mechanisms of JO treatment and discovered its ability

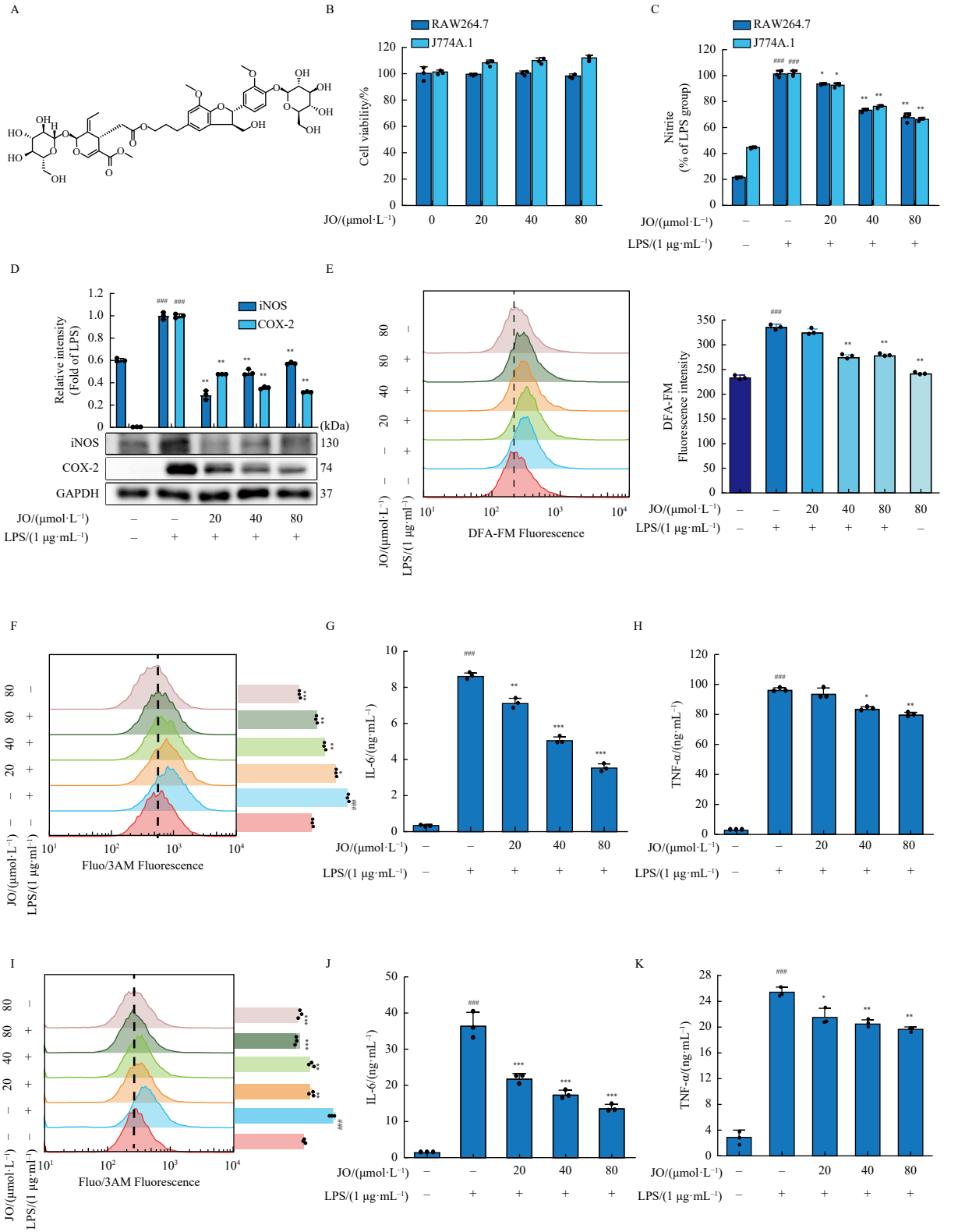

Fig. 1 JO inhibits inflammatory mediator release in macrophages. (A) Chemical structure of JO. (B) Cytotoxicity of JO (0, 20, 40, and 80 μmol·L^{-1}) in RAW264.7 and J774A.1 cells was assessed by MTT assay. (C) Nitrite concentrations in culture supernatants were measured using the Griess reagent. (D) Western blotting analysis of iNOS and COX-2 protein expressions in RAW264.7 cells. (E) Intracellular nitric oxide levels were quantified by flow cytometry using the DAF-FM probe in RAW264.7 cells. (F, I) Flow cytometry was also used to evaluate the Ca^{2+} level in RAW264.7 (F) and J774A.1 (I) cells treated with Fluo-3AM. (G, H, J, K) Levels of TNF-α and IL-6 in the culture supernatants of RAW264.7 (G, H) and J774A.1 (J, K) cells. The results are presented as the mean ± SD (n = 3). $^{###}P < 0.001$ *vs* the control group; $^{*}P < 0.05$, and $^{**}P < 0.01$ *vs* the LPS group.

to modulate the Nrf2/NF-κB/MAPKs signaling pathway, suppress inflammasomes, including NLRP3, and target TLR4 to prevent its dimerization. Additionally, JO regulated elevated inflammatory cytokines associated with ALI, such as tumor necrosis factor α (TNF-α) and IL-6 levels. Intravenous administration of JO to ALI-infected mice demonstrated reduced TLR4 expression and inflammatory responses, indicating JO's therapeutic potential in ALI treatment.

2. Materials and methods

2.1. Reagents

JO (> 98%) was isolated from *I. pubescens* var. *kwangsiensis* and characterized through HLPC analysis in our laboratory. The reagents utilized in this study, including MTT, Griess reagent (modified-G4410), $DCFH_2$-DA, LPS (*Escherichia coli*, serotype 0111: B4), TAK-242, JC-1, Fluo-3/AM, and DAF-FM, were acquired from Sigma-Aldrich (St. Louis, MO, USA). Furthermore, Pierce™ protein A/G magnetic beads (#88802) and Pierce™ anti-HA magnetic beads (#88836) were sourced from Thermo Fisher Scientific. Dulbecco's modified Eagle medium (DMEM) and fetal bovine serum (FBS) were obtained from Gibco (Grand Island, NY, USA). Antibodies against COX-2 (#4842), iNOS (#13120), p65 (#8242T), p-p65 (#3033), heme oxygenase-1 (HO-1) (#70081), Keap-1 (#4678), MyD88 (#4283), TLR4 (#14358), IKK-α (#2682), IKK-β (#8943T), p-(IKK)-α/β (#2078), IκB-α (#4814), p-IκB-α (#2859), cleaved-IL-1β (#63124), p-JNK1/2 (#4668T), JNK1/2 (#9252T), ERK1/2 (#4695T), poly (ADP-ribose) polymerase (PARP) (#9532), NLRP3 (#15101), IL-1β (#31202), cleaved-Caspase-1 (#89332), p-ERK1/2 (#4370T), p38 MAPK (#9212), GAPDH (#5174), p-p38 MAPK (#4511), Nrf2 (#12721), HA (#5017), and Flag (#14793) were acquired from Cell Signaling Technology (Beverly, MA, USA). Additional antibodies against NQO-1 (ab80588) and Caspase-1 (ab1872) were obtained from Abcam (Cambridge, MA, USA). Enzyme-linked immunosorbent assay (ELISA) kits for IL-6, IL-1β, and TNF-α were sourced from Neobioscience (Shenzhen, China), while the Nuclear and Cytoplasmic Protein Extraction kit was obtained from Beyotime (Shanghai, China).

2.2. Cell culture

The RAW264.7 cells used in this study were obtained from the Cell Bank of the Chinese Academy of Sciences (Shanghai, China), while the J774A.1 cell was acquired from the BeiNa Culture Collection (Jiangsu, China). The cells were cultured in DMEM supplemented with 10% FBS and maintained at 37 °C with 5% CO_2.

2.3. Cell viability assay

RAW264.7 and J774A.1 cells were exposed to JO (0, 20, 40, 80 μmol·L^{-1}) for 24 h. MTT solution (5 mg·mL^{-1}) was introduced to each well and incubated for an additional 3 h at 37 °C in the dark. Following supernatant removal, the cells were solubilized in DMSO (100 μL/well), and absorbance was measured using a microplate reader at 570 nm.

2.4. Griess reagent assay

RAW264.7 and J774A.1 cells underwent pretreatment with JO at concentrations of 0, 20, 40, and 80 μmol·L^{-1} for 1 h, followed by treatment with or without LPS at 1 μg·mL^{-1} for 18 h. The nitrite concentration in the supernatant was determined using the Griess reagent.

2.5. Flow cytometry

RAW264.7 and J774A.1 cells were treated with JO at various concentrations (0, 20, 40, 80 μmol·L^{-1}) for 1 h, followed by stimulation with or without LPS (1 μg·mL^{-1}) for 6 h. The fluorescence intensities of ROS detector $DCFH_2$-DA (1 μmol·L^{-1}), nitric oxide (NO) detector DAF-FM (0.5 μmol·L^{-1}), and Ca^{2+} detector Fluo-3/AM (1 μmol·L^{-1}) were analyzed using a flow cytometer (Becton-Dickinson, Franklin Lakes, NJ, USA).

2.6. ELISA

The cells underwent pretreatment with JO at varying concentrations (0, 20, 40, 80 μmol·L^{-1}) for 1 h, followed by LPS stimulation (1 μg·mL^{-1}) for 18 h. IL-6, IL-1β, and TNF-α levels were measured using ELISA kits according to the manufacturer's protocols.

2.7. Immunofluorescence

The cells received pretreatment with JO (80 μmol·L^{-1}) before LPS stimulation (1 μg·mL^{-1}). After treatment, the cells were incubated with anti-NF-κB/p65 antibody (1 : 100) overnight at 4 °C, followed by goat anti-rabbit Alexa Fluor 568 secondary antibody (1∶200) for 1 h at room temperature. Subsequently, the cells were fixed and stained with Hoechst 33342 (1 μmol·L^{-1}) for 30 min prior to imaging. The immunofluorescence analysis of Caspase-1 and Nrf2 followed the same protocol as NF-κB/p65. Images were captured using a confocal laser microscope (Leica, Wetzlar, Germany).

2.8. Live cell imaging

RAW264.7 cells received pretreatment with JO (80 μmol·L^{-1}) for 1 h, followed by stimulation with or without LPS. Following 30 min of staining with JC-1 (10 μg·mL^{-1}) and $DCFH_2$-DA (100 μmol·L^{-1}), fluorescence images were obtained using a fluorescence microscope (Leica, DMi8, Wetzlar, Germany).

2.9. TLR4 dimer formation

HA-TLR4 and Flag-TLR4 plasmids (Addgene, Watertown, Massachusetts, USA) were transfected into HEK293T cells using TurboFect transfection reagents according to the manufacturer's protocols. The transfected cells were plated in a 5 cm diameter dish and incubated overnight. The cells received pretreatment with JO (80 μmol·L^{-1}) before LPS stimulation (1 μg·mL^{-1}). Following stimulation, cells were harvested with IP lysis buffer, and TLR4 dimer formation was evaluated through Western blotting analysis using anti-HA magnetic beads.

2.10. Western blotting analysis

RAW264.7 and J774A.1 cells received pretreatment with various JO concentrations (0, 20, 40, or 80 μmol·L^{-1}) at specific time points, followed by LPS stimulation for a designated period. Proteins were extracted using RIPA lysis buffer. Immunoprecipitated samples were eluted with sodium dodecyl sulfate-polyacrylamide gel electrophoresis (SDS-PAGE) reducing sample buffer. The denatured proteins underwent separation by 8%, 10%, or 12% SDS-PAGE and transfer onto a polyvinylidene fluoride (PVDF) membrane (Millipore, Billerica, MA, USA) for Western blotting analysis. PVDF membranes were blocked with 5% non-fat milk for 2 h and incubated with primary antibodies (1∶1000) for 12 h at 4 °C and secondary antibodies (1∶5000) for 2 h at room temperature. Protein band signals were detected using SuperSignal West Femto maximum sensitivity substrate (Pierce Biotechnology, USA) and visualized using a ChemiDoc MP Imaging System (Bio-Rad, Hercules, CA, USA).

2.11. Cellular thermal shift assay

Following treatment with JO (80 μmol·L^{-1}), cells underwent lysis using RIPA lysis buffer, and total proteins were collected. The proteins were divided into 6 equal portions and heated at 44, 48, 52, 56, 60, and 64 °C for 3 min. Subsequently, loading buffer was added to the proteins, and protein levels were determined *via* Western blotting.

2.12. Docking of TLR4 dimerization

The TLR4 dimerization docking analysis was performed through molecular docking of JO with the TLR4-MD-2-LPS complex (PDB code: 3FXI) using Ledock (http://www.lephar.com). The TLR4-MD-2-LPS complex structures were obtained from the RCSB Protein Data Bank (PDB code: 3FXI).

2.13. Surface plasmon resonance (SPR) analysis

SPR analysis was conducted using a Biacore X100 instrument equipped with a CM5 sensor chip. Recombinant human TLR4 was immobilized in parallel-flow channels of a CM5 chip using an amine-coupling kit. JO was dissolved in HBS-P, and various JO concentrations were injected into the flow system at a rate of 30 L·min^{-1}. The association and dissociation times were set to 200 sec and 300 sec, respectively. Binding kinetics were analyzed using Biacore X100 Control Software 2.0.2.

2.14. Animal and experimental design

This study received approval from the Animal Policy and Welfare Committee of the Guangxi University of Chinese Medicine (Approval Document No. SYXK-GUI-2019-0001, 20190718), and all animal care and experiments adhered to the Local Guide for the Care and Use of Laboratory Animals. Male BALB/c mice weighing 18–22 g were obtained from Hunan SJA Laboratory Animal Co., Ltd. (Changsha, Hunan, China) and maintained under specific pathogen-free (SPF) conditions at a controlled temperature of 25 °C and humidity of 50%. The ALI model involved randomly assigning mice to different groups, including the control group, LPS group (4 or 15 mg·kg^{-1}; intratracheally, i.t.), JO administration groups (2.5, 5, and 10 mg·kg^{-1}, intravenously, i.v.), and positive control groups (dexamethasone; DEX; 5 mg·kg^{-1}, intraperitoneally, i.p.) with 10 mice per group (Yang et al., 2011). Control group mice received sterile saline. The mice were anesthetized with pentobarbital sodium (0.14 mL/10 g, i.p.) followed by noninvasive LPS administration into the lung tissue (4 or 15 mg·kg^{-1}; i.t.). For the JO-treated group, mice received JO preconditioning 2 h before LPS intratracheal instillation, with subsequent JO administrations at 2, 6, and 12 h. At 24 h post-LPS treatment, serum, bronchoalveolar lavage fluid (BALF), and lung tissue samples were collected and stored. Cytokine levels in serum and BALF samples were measured using TNF-α, IL-6, and IL-1β ELISA kits. ELISA kits also measured cytokine levels in lung homogenates. Lung tissue portions were fixed in 4% paraformaldehyde and embedded in paraffin for histological analysis. The remaining lung tissue was utilized for protein level measurement *via* Western blotting. Survival rates were monitored for 144 h following lethal LPS dose administration.

2.14.1. BALF collection

BALF collection involved inserting a catheter into the main bronchus through endotracheal intubation, followed by cold saline intubation. Approximately 0.8 ml of BALF was collected and centrifuged at 3000 × *g* for 15 min at 4 °C. The supernatant was immediately stored at −80 °C.

2.14.2. Histopathological examination

Following euthanization, mouse lung tissues were extracted and fixed in 4% formaldehyde solution for more than 24 h. The tissues underwent dehydration, paraffin embedding, and sectioning. The sections were then stained with HE. Histopathological examination involved observing and photographing the stained slides under a light microscope. TLR4 and p-p65 expression analysis was conducted through immunohistochemistry using rabbit anti-mouse TLR4 and p-p65 antibodies.

2.14.3. Hematology analysis

Blood samples were collected from the orbital region of the mice and treated with EDTA. A Mindray auto hematology analyzer, manufactured in Shenzhen, China, was employed to determine white blood cell (WBC), lymphocyte, and neutrophil counts.

2.14.4. Assessment of respiratory mechanics

Following LPS treatment, the mice were anesthetized and underwent tracheal incision. A 2 mm rigid casing was inserted and secured into the trachea, with the catheter connected to a small animal ventilator (Bestlab, Beijing, China). Mechanical ventilation was maintained at 90 breaths/min, with a tidal volume (VT) of 10 mL·kg^{-1} and a positive end-expiratory pressure of 5 cm H_2O established by a water column. The assessment included lung resistance (RL), expiration resistance (Re), and respiratory lung compliance (Cdyn).

2.14.5. Flow cytometry analysis

The single-cell suspensions from lung tissues underwent filtration after resuspension for cell counting and concentration adjustment. The cells were labeled with biomarkers PE-Cy™7 rat anti-CD11b (#25-0112-82, eBiosience) and BV421 rat anti-mouse F4/80 (#565411, BD Biosciences) for flow cytometry analysis. Flow cytometry results demonstrated that JO treatment reduced macrophage numbers in lung tissues compared to the model group.

2.15. Data analysis

All experiments were performed independently at least three times, and results are expressed as mean ± SD. Statistical analysis was conducted using GraphPad Prism 6.0 software (Microsoft, Seattle, WA, USA) with one-way ANOVA and Dunnett's multiple comparisons tests. Statistical significance was defined as $^{*}P < 0.05$, $^{**}P < 0.01$, and $^{***}P < 0.001$.

3. Results

3.1. JO inhibited inflammatory responses in macrophages

JO (20, 40, and 80 μmol·L^{-1}) exhibited no cytotoxicity in RAW264.7 or J774A.1 cells (Fig. 1B). JO effectively reduced LPS-induced nitrite levels in both cell lines (Fig. 1C) and markedly decreased iNOS and COX-2 protein expression in RAW264.7 cells (Fig. 1D). Additionally, JO inhibited NO production in RAW264.7 cells (Fig. 1E). ELISA results indicated that JO decreased IL-6 and TNF-α levels in RAW264.7 cells (Figs. 1G and 1H) and reduced the intracellular calcium concentration in LPS-induced RAW264.7 cells (Fig. 1F). Comparable effects were observed in J774A.1 cells, where JO decreased intracellular calcium concentration and IL-6 and TNF-α secretion (Figs. 1I, 1J, and 1K). These results demonstrate JO's substantial anti-inflammatory properties.

3.2. JO regulated oxidative stress responses in macrophages

Flow cytometry and ROS assays confirmed that JO decreased

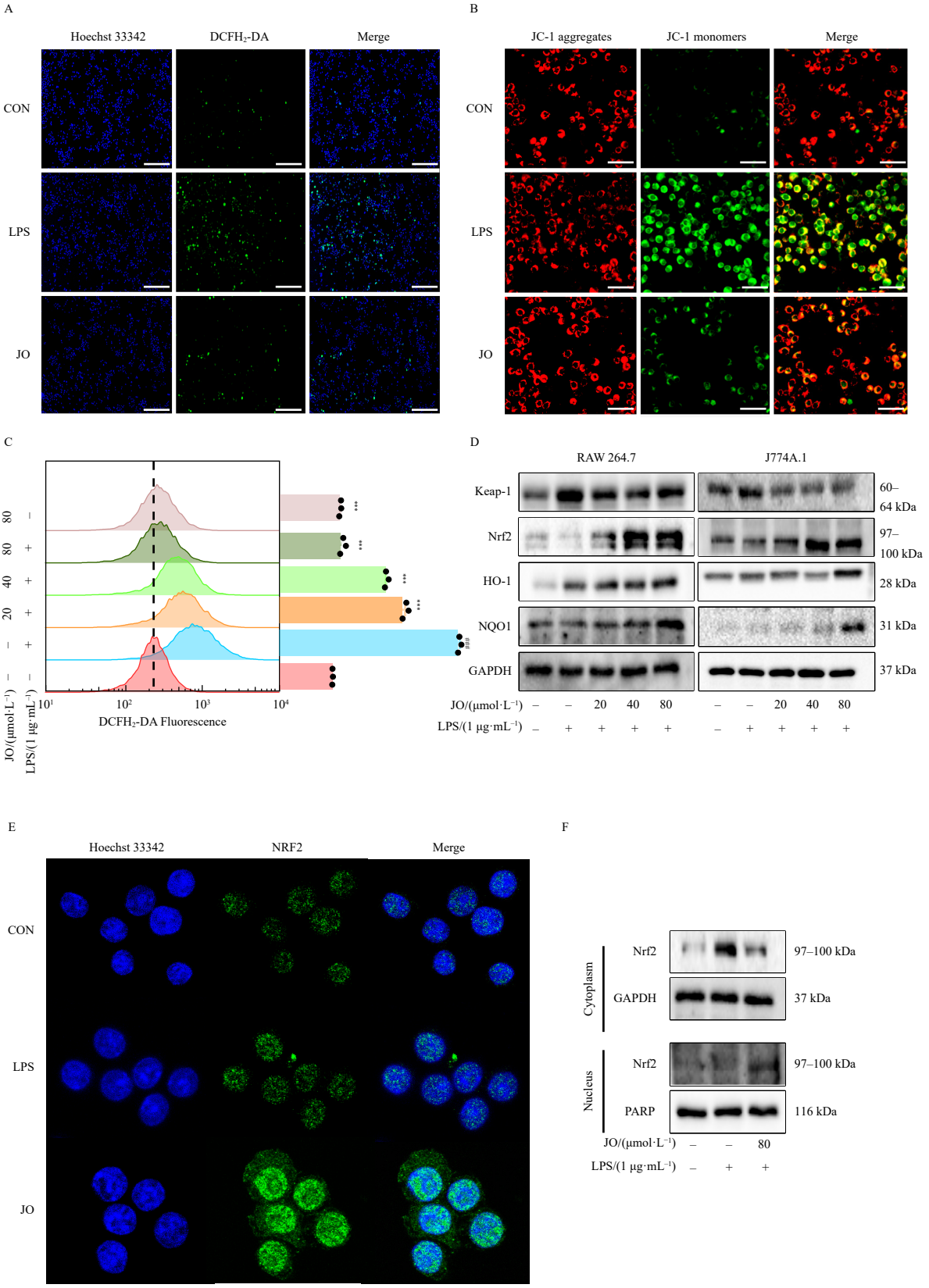

Fig. 2 JO regulates oxidative stress responses in macrophages. (A) RAW 264.7 cells were stained with $DCFH_2$-DA and imaged using a fluorescence microscope (scale bar = 10 μm). (B) The mitochondrial membrane potential (MMP) was detected using JC-1 (mitochondrial membrane potential probe) and imaged using a fluorescence microscope in RAW 264.7 cells (scale bar = 10 μm). (C) Quantification of intracellular ROS levels by flow cytometry following DCFH2-DA staining in RAW264.7 cells. (D) The protein expression levels of Keap1, Nrf2, HO-1, and NQO1 in RAW 264.7 and J774A.1 cells were detected by Western blotting. (E) Nrf2 translocation in RAW 264.7 cells was visualized *via* fluorescence staining (scale bar = 10 μm). (F) The protein expression of Nrf2 in the cytoplasmic and nuclear fractions of RAW 264.7 cells was detected by Western blotting. Data are presented as the mean ± SD (n = 3). $^{###}P < 0.001$ *vs* the control group; $^{*}P < 0.05$ and $^{***}P < 0.001$ *vs* the LPS group.

ROS production in LPS-induced RAW264.7 cells (Figs. 2A and 2C). JO pretreatment restored LPS-disrupted mitochondrial membrane potential (MMP) in RAW264.7 cells (Fig. 2B). In LPS-induced RAW264.7 and J774A.1 cells, JO enhanced Nrf2, HO-1, and NQO1 protein expression while suppressing Keap1 (Fig. 2D). JO promoted Nrf2 nuclear translocation, decreasing its cytoplasmic expression while increasing nuclear expression (Fig. 2F), as verified by immunofluorescence analysis (Fig. 2E). These findings demonstrate JO's capacity to inhibit ROS production, restore MMP, and facilitate Nrf2 translocation in macrophages.

3.3. NLRP3 inflammasome activation in macrophages inhibited by JO

The NLRP3 inflammasome serves a crucial role in inflammatory diseases [16]. To examine the effect of JO on NLRP3 inflammasome activation, we assessed the expression of NLRP3 inflammasome-related proteins, including NLRP3, ASC, Caspase-1, and IL-1β. As illustrated in Figs. 3A and 3B, the expression of NLRP3, cleaved Caspase-1, and LPS/ATP elevated cleaved IL-1β was markedly decreased by JO pretreatment. The IL-1β level in the supernatant was determined using ELISA, which demonstrated consistent results with protein expression (Fig. 3C). Additionally, JO treatment inhibited Caspase-1 activation in LPS + ATP-treated cells (Fig. 3D). These results suggest that JO can inhibit NLRP3 inflammasome activation.

3.4. The NF-κB and MAPK pathways were involved in the anti-inflammatory effects of JO on macrophages

The NF-κB signaling pathway functions as a key regulator of the inflammatory response [17]. In LPS-induced cells, including RAW264.7 and J774A.1 cells, the expression of proteins associated with the NF-κB signaling pathway, such as p-IκB-α, p-IKKα/β, and p-p65, increased. However, JO substantially reduced

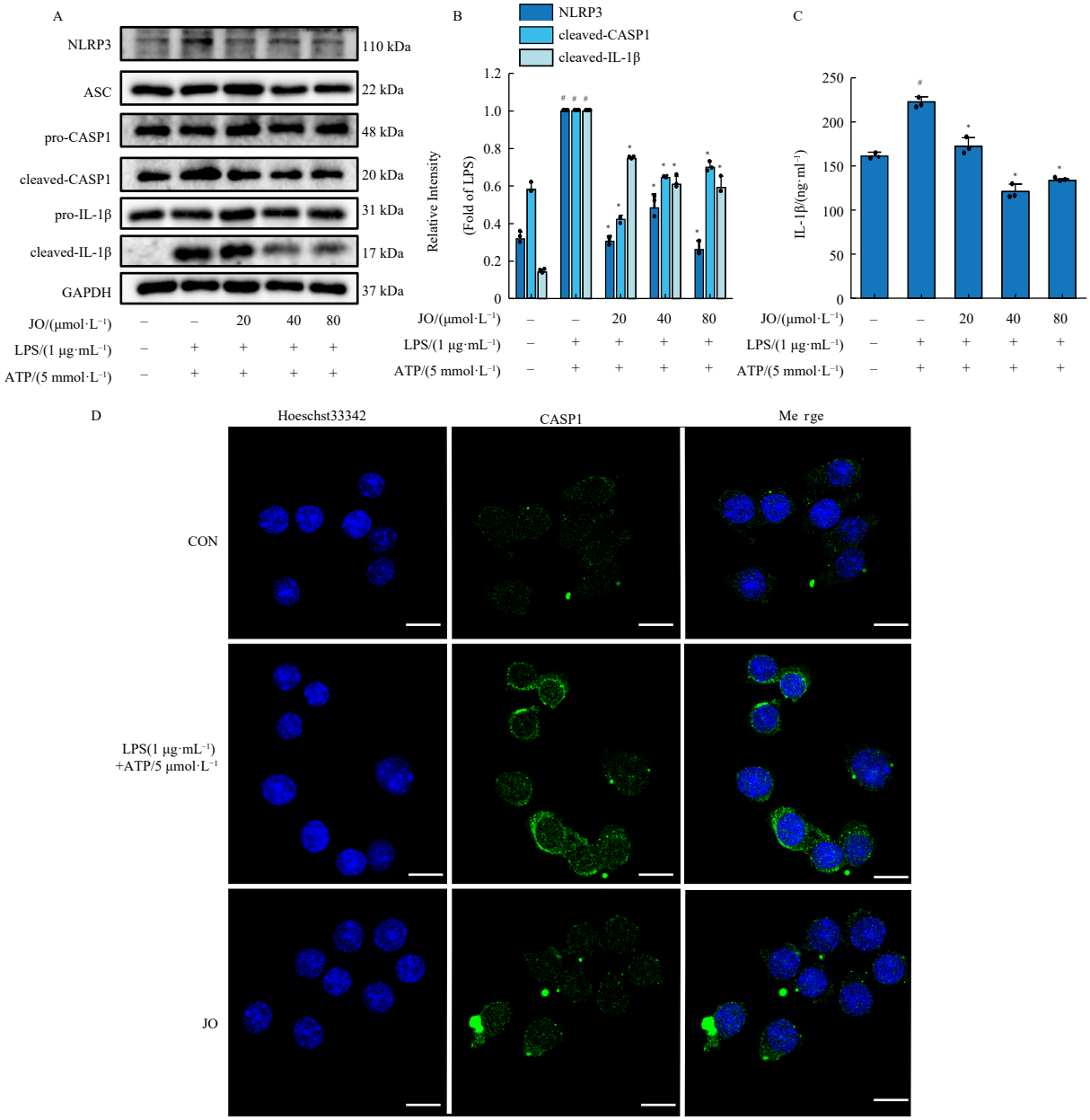

Fig. 3 JO inhibits NLRP3 inflammasome activation and IL-1β secretion in J774A.1 cells. (A–B) Western blotting analysis of the protein expression levels of NLRP3, ASC, pro-caspase-1 (CASP1), cleaved CASP1, pro-IL-1β, and cleaved IL-1β. (C) Secretion of IL-1β into the culture supernatant was measured by ELISA. (D) Activation of cleaved caspase-1 activation was visualized by immunofluorescence staining (scale bar = 10 μm). Data are presented as the mean ± SD (n = 3). $^{\#}P < 0.05$ *vs* the control group; $^{*}P < 0.05$ *vs* the LPS + ATP group.

the expression of these proteins, as demonstrated in Fig. 4A. LPS triggers the nuclear translocation of NF-κB/p65, which enhances the transcription and expression of pro-inflammatory cytokines and inflammation-related enzymes, subsequently inducing an inflammatory response [17]. JO inhibited the nuclear translocation of NF-κB/p65, as shown in Fig. 4C and validated by the immunofluorescence results in Fig. 4D. The MAPK pathway, activated by LPS, also maintains a significant role in inflammation [18]. MAPKs participate in the LPS-mediated production of TNF-α and IL-6 [19]. As illustrated in Fig. 4B, JO significantly decreased the phosphorylation of p38 MAPK, JNK1/2, and ERK1/2. These findings indicate that JO exhibits anti-inflammatory effects through the NF-κB and MAPK pathways.

3.5. JO binding to TLR4

TLR4 regulates the activation of the NLRP3 inflammasome [20]. Administration of the TLR4 inhibitor TAK242 markedly reduced the protein expression of NLRP3. These observations indicate that TLR4 serves an essential function in the activation of the NLRP3 inflammasome (Fig. 5A). JO suppressed TLR4 and MyD88 protein expression in RAW264.7 and J774A.1 cells (Fig. 5B). JO diminished TLR4 dimerization in HEK293T cells (Fig. 5C) and attenuated TLR4 and MyD88 complex formation in RAW264.7 cells (Fig. 5D). Molecular docking and SPR analyses confirmed the direct binding of JO to TLR4 (Figs. 5F–5J). The predicted binding energy between JO and TLR4 is −32.85 kJ·mol^{-1}. JO establishes favorable interactions with residues including ASN 282, ILE 285, CYS 306, ASN 309, LEU 283, GLU 225, MET 201, LEU 198, ARG 227, and GLU 254 (Fig. 5G). A cellular thermal shift assay verified the direct binding of JO to TLR4 (Fig. 5H), which was subsequently confirmed by an SPR assay using a Biacore platform. The equilibrium dissociation constant (Kd) for JO binding to the TLR4 protein was approximately 35.1 μmol·L^{-1} (Fig. 5I and J),

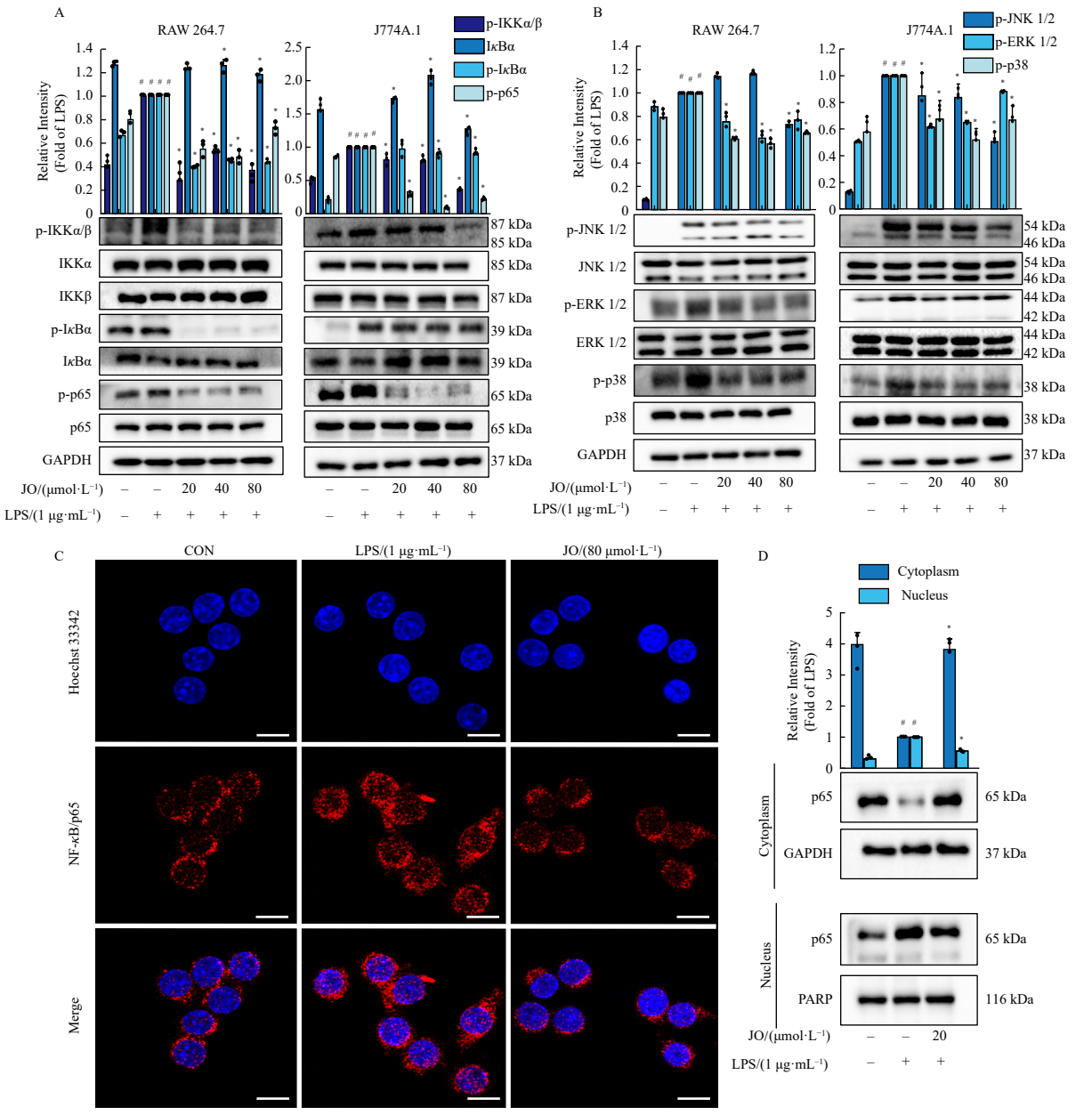

Fig. 4 The NF-κB and MAPK pathways were involved in the anti-inflammatory effects of JO on macrophages. (A) Western blotting analysis of phosphorylated and total protein levels of p-IKKB kinase (IKK)-α/β, IKK-α, IKK-β, p-IκB-α, IκB-α, p-p65/NF-κB, and p65/NF-κB. (B) Western blotting analysis of phosphorylated and total protein levels of p-JNK1/2, JNK1/2, ERK1/2, p-ERK1/2, p-38 MAPK, and p-p38 MAPK following JO treatment and LPS stimulation. (C–D) RAW264.7 cells were pretreated with JO and then stimulated with LPS. (C) Immunofluorescence images showing p65 translocation by JO in RAW 264.7 cells (scale bar = 10 μm). (D)Western blotting analysis of p65 expression in cytoplasmic and nuclear fraction. Data are presented as the mean ± SD (n = 3). $^{\#}P < 0.05$ *vs* the control group. $^{*}P < 0.05$ *vs* the LPS group.

demonstrating a significant interaction between JO and TLR4. These results suggest that JO mediates its anti-inflammatory effects through binding to TLR4.

3.6. JO ameliorated LPS-induced ALI in mice

This study investigated the mechanisms underlying the therapeutic effects of JO administration on ALI *in vivo*. Initially, mice received a lethal dose of LPS administered noninvasively to lung tissue, followed by treatment with or without JO. The mice were monitored for 120 h. The LPS group showed 0% survival at 84 h, while the DEX group maintained an 80% survival rate from 84 to 120 h. Both JO (5 mg·kg^{-1}) and JO (10 mg·kg^{-1}) groups demonstrated improved survival rates from 84 to 120 h (Fig. 6A). JO administration reduced lung RL and Re (Sup Figs. 1A, 1B) while enhancing lung Cdyn (Sup Fig. 1C). H&E staining demonstrated that JO mitigated LPS-induced lung tissue damage (Fig. 6B). The findings indicated that LPS increased WBC, neutrophil, and lymphocyte counts in mouse blood, whereas JO pretreatment significantly reduced these parameters (Figs. 6C–6E). Furthermore, JO significantly inhibited TNF-α, IL-6, and IL-1β release in the BALF (Figs. 6F–6H). Similar patterns were observed in serum and lung tissues (Sup Figs. 1D–1I). Flow cytometry analysis further demonstrated JO's impact on lung macrophage populations: the control group exhibited 5.04% F4/80-positive macrophages, which increased to 11.8% following LPS administration. Treatment with JO (5 mg·kg^{-1}) reduced this proportion to 8.69%, while 10 mg·kg^{-1} JO further decreased it to 6.61%, comparable to the DEX group at 6.85% (Sup Fig. 1K), indicating attenuation of inflammatory cell infiltration. Immunohistochemistry demonstrated that JO decreased TLR4 and p-p65 expression sin lung tissues (Figs. 6I–6J), findings that were corroborated by Western blotting (Sup Fig. 1K). These results suggest that JO ameliorates LPS-induced ALI in mice by suppressing inflammatory cell infiltration and cytokine production while inhibiting the TLR4/NF-κB signaling pathway.

4. Discussion

ALI represents a severe condition characterized by deteriorating lung function and high mortality rates due to uncontrolled inflammatory responses [21]. Recent research indicates that ALI pathogenesis involves early alveolar inflammation concurrent with lung injury [22]. Pathogenic microorganisms activate lung tar-

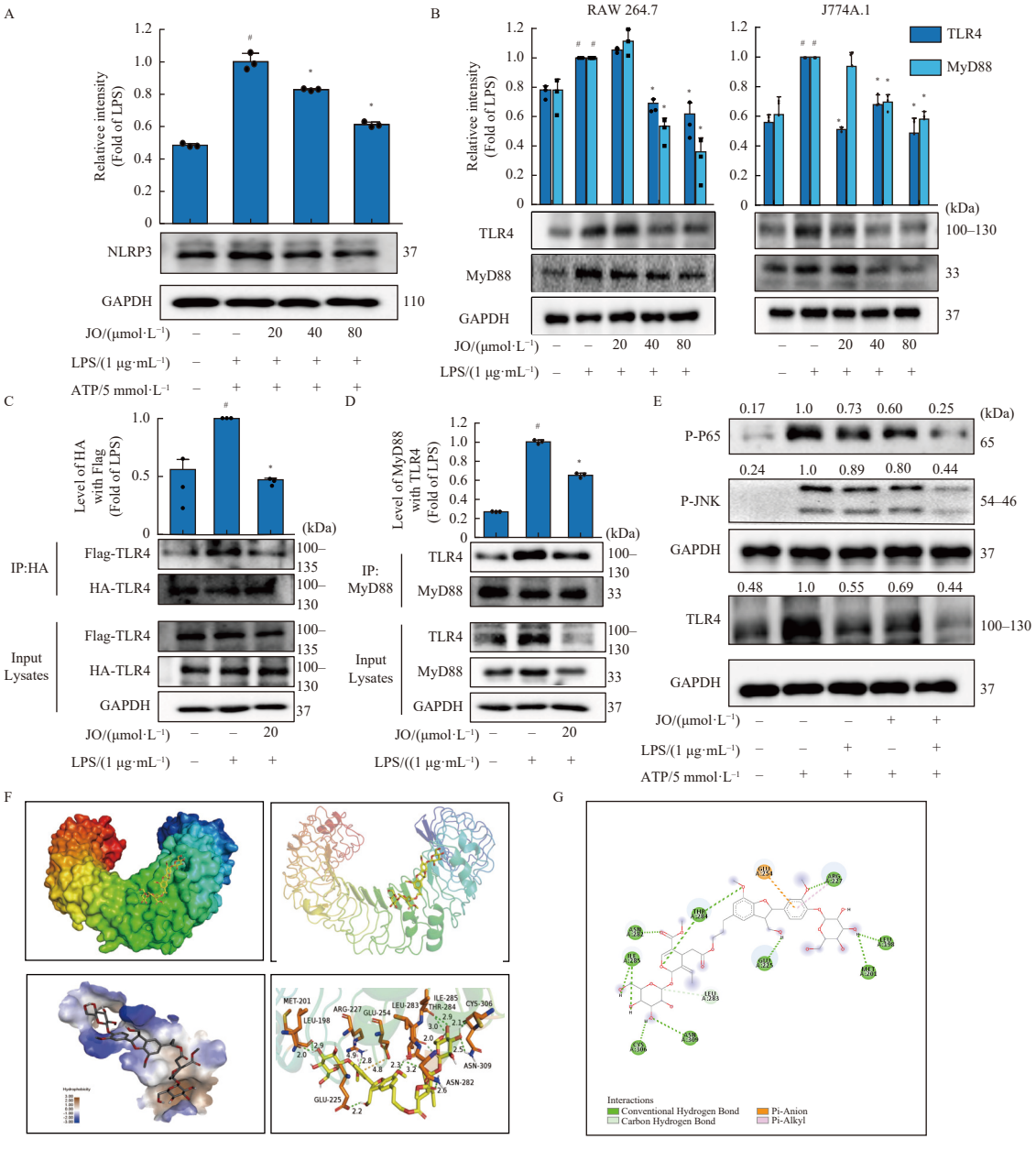

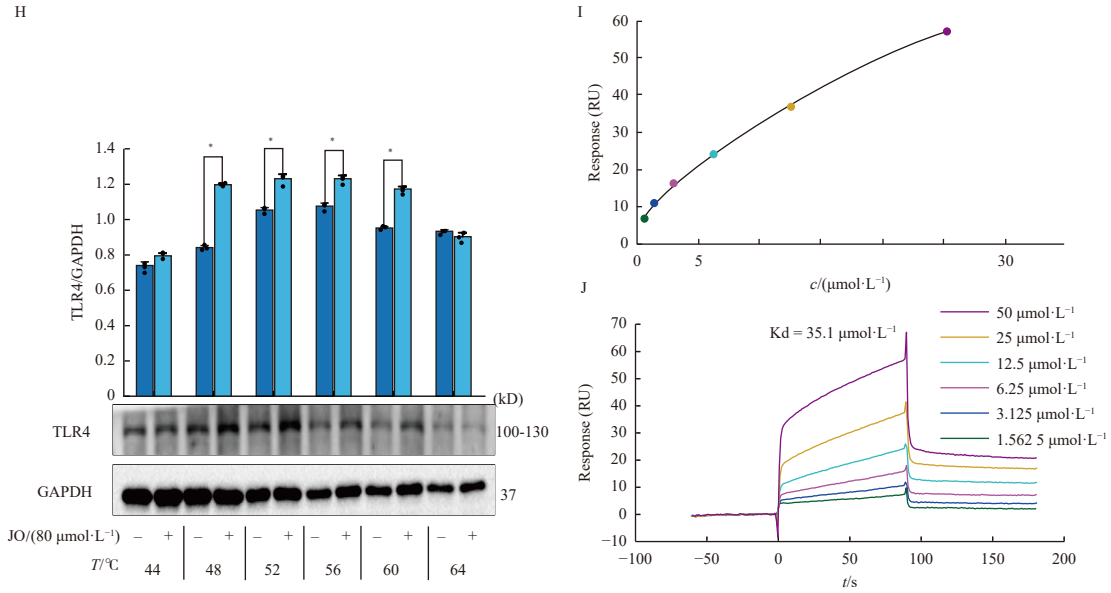

Fig. 5 JO inhibits LPS-induced TLR4-MyD88) complex formation. (A) J774A.1 cells were pretreated with TAK242 before being stimulated with LPS and ATP. NLRP3 protein levels were analyzed by Western blotting, with representative bands and quantitative graphs shown. (B) Western blotting analysis of TLR4 and MyD88 protein expressions in RAW264.7 and J774A.1 cells. (C) HEK293T cells were cotransfected with TLR4-HA and TLR-Flag plasmids, pretreated with JO, and then stimulated with LPS. TLR4 dimerization was assessed by co-immunoprecipitation with anti-HA magnetic beads, followed by Western blotting detection. (D) RAW264.7 cell lysates were immunoprecipitated using anti-MyD88 magnetic beads, and associated proteins were detected by Western blotting to evaluate TLR4-MyD88 complex formation. (E)Western blotting analysis of P-P65, P-JNK, and TLR4 levels in RAW264.7 cells. (F-G) Molecular docking of JO with the TLR4-MD2 complex. The chemical structure of JO is shown in the docking pocket. TLR4 and MD2 are shown in pink and gray, respectively, and their dimerization partners are shown in yellow and gray, respectively. (H) Cellular thermal shift assay: RAW264.7 cell lysates treated with JO were heated to 44, 48, 52, 56, 60, and 64 °C, and TLR4 stability was assessed by Western blotting. (I-J) SPR analysis of the binding between JO and immobilized recombinant human TLR4 on a CM5 sensor chip. Data are presented as the mean ± SD (n = 3). $^{\#}P < 0.05$ *vs* the control group; $^{*}P < 0.05$ *vs* the LPS group.

get cells, triggering the secretion of TNF-α, IL-1β, and IL-6. These activated cytokines subsequently stimulate endothelial cells, leading to pulmonary edema [23]. TLR4 functions as a receptor that responds to inflammatory stimuli through LPS binding. This interaction promotes TLR4 dimer formation, which activates downstream NF-κB and MAPK signaling pathways *via* the MyD88 protein [3]. The NF-κB/MAPK signaling pathway demonstrates inhibitory effects on inflammatory factors, including TNF-α and IL-6, playing a significant role in LPS-induced ALI development [24]. In macrophages exposed to LPS and ATP, intracellular ROS balance disruption activates the NLRP3 inflammasome [10, 25]. NLRP3 inflammasome inhibition presents a potential therapeutic approach for ALI, as its activation results in cleaved Caspase-1 and mature IL-1β overexpression, promoting neutrophil recruitment and ALI progression [26]. Thus, suppressing NLRP3 inflammasome activation represents a promising therapeutic strategy for ALI treatment.

Research indicates that TLR4 interacts with LPS, forming a polymer TLR4-LPS complex that initiates pro-inflammatory signaling pathways [27, 28]. Consequently, preventing TLR4 dimerization represents a potential therapeutic strategy for disease management [5]. Through molecular docking and SPR assays, this study demonstrates that JO binds to TLR4, thereby inhibiting TLR4 dimer formation. Following TLR4 activation, MyD88 recruitment activates the NF-κB and MAPK pathways, triggering inflammatory cytokine release [29]. The present study reveals that JO substan-

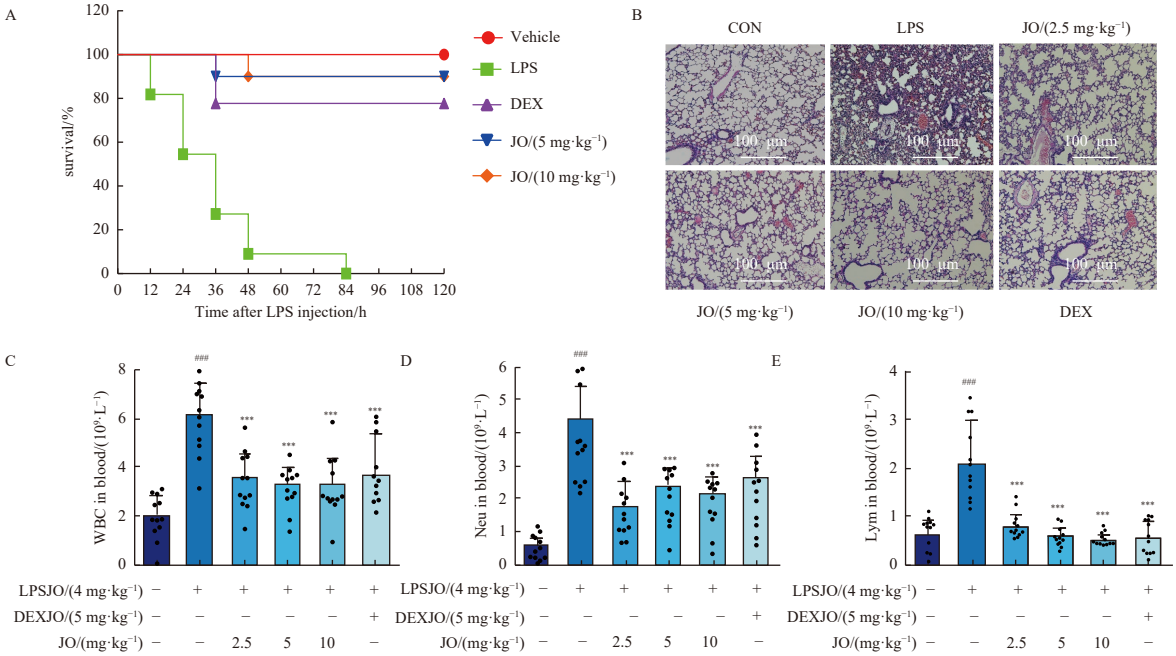

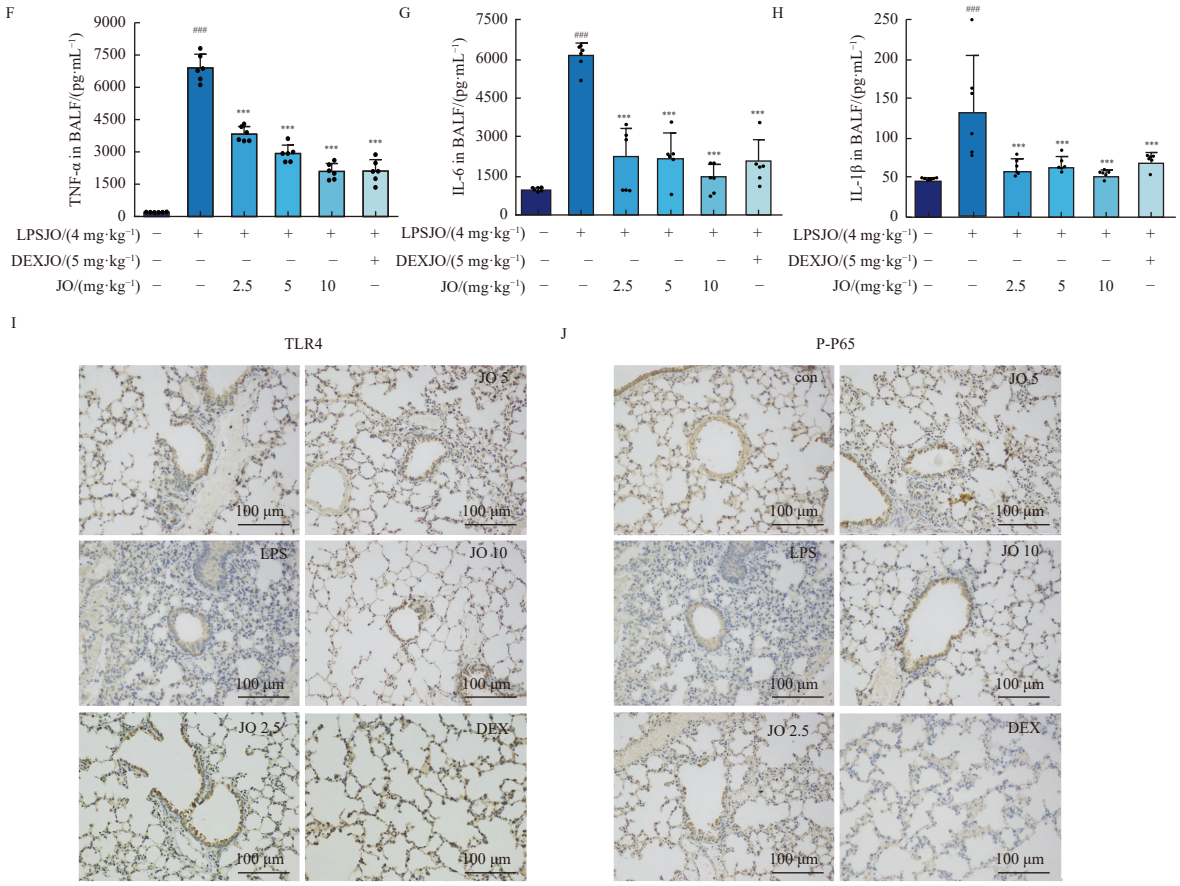

Fig. 6 JO ameliorates LPS-induced ALI in mice. (A) Survival rates were monitored for 120 h (n = 10). (B) epresentative histopathological images of lung sections 24 h after LPS challenge (scale bar = 100 μm) (n = 6). (C) White blood cell (WBC), (D) neutrophil, and (E) lymphocyte counts were measured using an automated hematology analyzer (n = 12). (F-H) Levels of TNF-α, IL-6, and IL-1β in BALF were measured (n = 6). Immunohistochemical staining for (I) TLR4 and (G) p-p65 in the lung tissues of ALI mice. Positive immunoreactivity is indicated in brown (scale bar = 100 μm). Data are presented as the mean ± SD. $^{###}P < 0.001$ *vs* the control group; $^{*}P < 0.05$, $^{**}P < 0.01$, $^{***}P < 0.001$ *vs* the LPS group.

tially reduces TLR4 and MyD88 precipitation while inhibiting NF-κB/MAPK signaling pathway activation. Furthermore, under oxidative stress conditions, Nrf2 separates from Keap1, translocates to the nucleus, and binds to the antioxidant response element (ARE) to initiate HO-1 transcription [30].

The NLRP3 inflammasome serves an essential function in the immune system, facilitating host immune defence and inflammatory responses against pathogenic microorganisms, including bacteria, fungi, and viruses [31]. NLRP3 inflammasome activation involves two distinct phases: priming and activation. During the priming phase, inflammatory stimuli such as TLR4 agonists induce NLRP3 and pro-IL-1β expression through NF-κB signaling. The activation phase is initiated by PAMPs and DAMPs, resulting in NLRP3 inflammasome assembly and IL-1β/18 secretion through Caspase-1-mediated pathways. Research has demonstrated that the activation phase is influenced by ROS generation, which promotes NLRP3 inflammasome activation and inflammatory cascade reactions. The current study demonstrates that JO effectively reduces NLRP3 expression, Caspase-1 cleavage, and IL-1β secretion in macrophages, aligning with previous research findings.

Prior research has established that Nrf2 activation induces the transcription of AREs, including HO-1, which reduces ROS production and subsequent inflammasome activation [12, 21, 32]. ROS reduction particularly affects the regulation of the NLRP3 inflammasome, a multiprotein complex essential to innate immune response. Increased ROS levels trigger NLRP3 inflammasome activation, promoting inflammation [33]. Through ROS reduction, Nrf2 activation suppresses NLRP3 inflammasome activation, thereby regulating inflammation [34]. This study demonstrates JO's significant effects on the Nrf2 pathway, ROS production, and NLRP3 inflammasome activation. JO reduces ROS production in LPS-induced RAW264.7 and J774A.1 cells, maintains MMP, and enhances Nrf2, HO-1, and NQO1 protein expression while suppressing Keap1. JO pretreatment markedly decreases NLRP3, cleaved Caspase-1, and IL-1β expression in LPS/ATP-stimulated J774A.1 cells. These findings suggest that JO inhibits NLRP3 inflammasome activation through ROS reduction and Nrf2 activation promotion. Additional research is necessary to directly validate this mechanistic pathway.

When pathogenic microorganisms are present, lung target cells become activated, secreting inflammatory cytokines including TNF-α, IL6, and IL-1β, which activate endothelial cells and induce pulmonary edema [35]. Research demonstrates that JO reduces inflammation by suppressing TNF-α, IL-6, and IL-1β secretion while limiting excessive neutrophil, lymphocyte, and leukocyte accumulation. TLR4 maintains a crucial role in immune response regulation by controlling NF-κB/p65 activation and subsequent inflammatory agent release. The study reveals that JO treatment significantly reduces TLR4 and p-p65 expression in lung tissues.

5. Conclusion

This study presents the first demonstration of JO's *in vitro* and *in vivo* anti-inflammatory properties. The findings reveal that JO provides protective effects against ALI in mice, with its mechanism potentially involving the NF-κB/MAPKs/Nrf2-NLRP3 in-

flammasome pathway through TLR4 binding. These results indicate that JO represents a potential therapeutic candidate for ALI treatment.

Funding

This work was supported by the National Natural Science Foundation of China (No. 82260799), Guangxi Science and Technology Base and Talent Project (No. AA23026010), Undergraduate Innovation and Entrepreneurship Training Program (No. S202110600120), Guangxi Overseas "100 Persons' Plan" High-level Expert, University of Chinese Medicine (No. 2022BS008), Guangxi University Young and Middle-aged Teachers Research Basic Ability Improvement Project (No. 2023KY0303), and Jiangxi Province 2022 Annual Graduate Student Innovation Special Fund Project (No. YC2022-B189).

Supporting information

Supporting information for this paper is available upon email request to thecorres-ponding authors.

Declaration of competing interest

The authors declare no competing financial interest.

References

1 Zhang J, Guo Y, Mak M, et al. Translational medicine for acute lung injury. *J Transl Med*. 2024;22:25. https://doi.org/10.1186/s12967-023-04828-7.
2 D'Alessio FR. Mouse models of acute lung injury and ARDS. *Methods Mol Biol*. 2018;1809:341-350. https://doi.org/10.1007/978-1-4939-8570-8_22.
3 Gao H, Kang N, Hu C, et al. Ginsenoside Rb1 exerts anti-inflammatory effects *in vitro* and *in vivo* by modulating toll-like receptor 4 dimerization and NF-κB /MAPKs signaling pathways. *Phytomedicine*. 2020;69:153197. https://doi.org/10.1016/j.phymed.2020.153197.
4 Yuan R, Huang L, Du LJ, et al. Dihydrotanshinone exhibits an anti-inflammatory effect *in vitro* and *in vivo* through blocking TLR4 dimerization. *Pharmacol Res*. 2019;142:102-114. https://doi.org/10.1016/j.phrs.2019.02.01.
5 Gao H, Cui Y, Kang N, et al. Isoacteoside, a dihydroxyphenylethyl glycoside, exhibits anti-inflammatory effects through blocking toll-like receptor 4 dimerization. *Br J Pharmacol*. 2017;174:2880-2896. https://doi.org/10.1111/bph.13912.
6 Wang F, Fu X, Wu X, et al. Bone marrow derived M2 macrophages protected against lipopolysaccharide-induced acute lung injury through inhibiting oxidative stress and inflammation by modulating neutrophils and T lymphocytes responses. *Int Immunopharmacol*. 2018;61:162-168. https://doi.org/10.1016/j.intimp.2018.05.015.
7 Han S, Li S, Li J, et al. Hederasaponin C inhibits LPS-induced acute kidney injury in mice by targeting TLR4 and regulating the PIP2/NF-κB/NLRP3 signaling pathway. *Phytother Res*. 2023;37:5974-5990. https://doi.org/10.1002/ptr.8014.
8 He J, Yuan R, Cui X, et al. Anemoside B4 protects against Klebsiella pneumoniae-and influenza virus FM1-induced pneumonia *via* the TLR4/Myd88 signaling pathway in mice. *Chin Med*. 2020;15:1-13. https://doi.org/10.1186/s13020-020-00350-w.
9 Liu Z, Zhao H, Liu W, et al. NLRP3 inflammasome activation is essential for paraquat-induced acute lung injury. *Inflammation*. 2015;38:433-444, https://doi.org/10.1007/s10753-014-0048-2.
10 Saghahazrati S, Ayatollahi SA, Kobarfard F, et al. Attenuation of inflammation in streptozotocin-induced diabetic rabbits by Matricaria chamomilla oil: a focus on targeting NF-κB and NLRP3 signaling pathways. *Chin Herb Med*. 2020;12:73-78, https://doi.org/10.1016/j.chmed.2019.12.003.
11 Cai W, Chen J. Herbs used in traditional Chinese medicine in treatment of heart diseases. In: *Bioactive Food as Dietary Interventions for Cardiovascular Disease*. Academic Press: Cambridge, MA, USA, 2013:551-590.
12 Hou XY, Liu YC, Du HZ. Potential role of Natural Herbal Tea as a healthy beverage in reducing the risk of liver cancer and chronic liver disease mortality. *Chin J Nat Med*. 2023;21(12): 884-885, https://doi.org/10.1016/S1875-5364(23)60507-2.
13 Jiang S, Cui H, Wu P, et al. Botany, traditional uses, phytochemistry, pharmacology and toxicology of *Ilex pubescens* Hook et Arn. *J Ethnopharmacol*. 2019;245:112147, https://doi.org/10.1016/j.jep.2019.112147.
14 Shen YC, Hsieh PW, Kuo YH. Neolignan glucosides from Jasminum urophyllum. *Phytochemistry*. 1998;48:719-723. https://doi.org/10.1016/j.jep.2017.02.013.
15 Huang YL, Oppong MB, Guo Y, et al. The Oleaceae family: a source of secoiridoids with multiple biological activities. *Fitoterapia*. 2019;136:104155, https://doi.org/10.1016/j.fitote.2019.04.010.
16 Han YH, Liu XD, Jin MH. et al. Role of NLRP3 inflammasome-mediated neuronal pyroptosis and neuroinflammation in neurodegenerative diseases. *Inflamm Res*. 2023;72:1839-1859, https://doi.org/10.1007/s00011-023-01790-4.
17 Yuan R, Li Y, Han S. et al. Fe-curcumin nanozyme-mediated reactive oxygen species scavenging and anti-inflammation for acute lung injury. *ACS Cent Sci*. 2021;8:10-21, https://doi.org/10.1021/acscentsci.1c00866.
18 Zhang X, Lian X, Li H, et al. Taxifolin attenuates inflammation *via* suppressing MAPK signal pathway *in vitro* and *in silico* analysis. *Chin Herb Med*. 2022;14:554-562, https://doi.org/10.1016/j.chmed.2021.03.002.
19 Yi G, Li H, Liu M. et al. Soybean protein-derived peptides inhibit inflammation in LPS-induced RAW264. 7 macrophages *via* the suppression of TLR4-mediated MAPK-JNK and NF-kappa B activation. *J Food Biochem*. 2020;44:e13289, https://doi.org/10.1111/jfbc.13289.
20 Ikenohuchi YJ, Silva MDS, Rego CMA, et al. A C-type lectin induces NLRP3 inflammasome activation *via* TLR4 interaction in human peripheral blood mononuclear cells. *Cell Mol Life Sci*. 2023;80:188, https://doi.org/10. 1007/s00018-023-04839-z.
21 Li ST, Jiang Y, Wang J, et al. HO-1/autophagic flux axis alleviated sepsis-induced acute lung injury *via* inhibiting NLRP3 inflammasome. *Cell Signal*. 2022;100:110473. https://doi.org/10.1016/j.cellsig.2022.110473.
22 Alluri R, Kutscher HL, Mullan BA, et al. Open tracheostomy gastric acid aspiration murine model of acute lung injury results in maximal acute nonlethal lung injury. *J Vis Exp*. 2017;120:e54700, https://doi.org/10.3791/54700.
23 Yuan R, He J, Huang L, et al. Anemoside B4 protects against acute lung injury by attenuating inflammation through blocking NLRP3 inflammasome activation and TLR4 dimerization. *J Immunol Res*. 2020:2020:7502301. https://doi.org/10.1155/2020/7502301.
24 Li XX, Yuan R, Wang QQ, et al. Rotundic acid reduces LPS-induced acute lung injury *in vitro* and *in vivo* through regulating TLR4 dimer. *Phytother Res*. 2021;35(8):4485-4498. https://doi.org/10.1002/ptr.7152.
25 Bai B, Yang Y, Wang Q, et al. NLRP3 inflammasome in endothelial dysfunction. *Cell Death Dis*. 2020:11:1-18. https://doi.org/10.1038/s41419-020-02985-x.
26 Ma Y, Wang Z, Wu X. et al. 5-Methoxytryptophan ameliorates endotoxin-induced acute lung injury in vivo and in vitro by inhibiting NLRP3 inflammasome-mediated pyroptosis through the Nrf2/HO-1 signaling pathway. *Inflammation Res*. 2023;72:1633-1647, https://doi.org/10.1007/s00011-023-01769-1.
27 Ryu JK, Kim SJ, Rah SH, et al. Reconstruction of LPS transfer cascade reveals structural determinants within LBP, CD14, and TLR4-MD2 for efficient LPS recognition and transfer. *Immunity*. 2017;46:38-50. https://doi.org/10.1016/j.immuni.2016.11.007.
28 Li L, Chen H, Huang G, et al. Structure of polysaccharide from *Dendrobium nobile* Lindl. and its mode of action on TLR4 to exert immunomodulatory effects. *Foods*. 2024;13:1356, https://doi.org/10.3390/foods13091356.
29 Kochumon S, Wilson A, Chandy B, et al. Palmitate activates CCL4 expression in human monocytic cells *via* TLR4/MyD88 dependent activation of NF-κB/MAPK/PI3K signaling systems. *Cell Physiol Biochem*. 2018;46:953-964, https://doi.org/10.1159/000488824.
30 Wen Z, Liu W, Li X, et al. A protective role of the NRF2-Keap1 pathway in maintaining intestinal barrier function. *Oxid Med Cell Longev*. 2019;2019:1759149. https://doi.org/10.1155/2019/1759149.
31 Yang CS, Shin DM, Jo EK. The role of NLR-related protein 3 inflammasome in host defense and inflammatory diseases. *Int Neurourol J*. 2012;16:2. https://doi.org/10.5213/inj.2012.16.1.2.
32 Jhang JJ, Yen GC. The role of Nrf2 in NLRP3 inflammasome activation. *Cell Mol Immunol*. 2017;14:1011-1012. https://doi.org/10.1038/cmi.2017.114.
33 Yazal T, Lee PY, Chen PR, et al. Kurarinone exerts anti-inflammatory effect *via* reducing ROS production, suppressing NLRP3 inflammasome, and protecting against LPS-induced sepsis. *Biomed Pharmacother*. 2023;167:115619. https://doi.org/10.1016/j.biopha.2023.115619.
34 Gao Y, Guo X, Zhou Y, et al. Kynurenic acid inhibits macrophage pyroptosis by suppressing ROS production *via* activation of the NRF2 pathway. *Mol Med Rep*. 2023;28:1-11. https://doi.org/10.3892/mmr.2023.13098.
35 Han S, Yuan R, Cui Y, et al. Hederasaponin C alleviates lipopolysaccharide-induced acute lung injury *in vivo* and *in vitro* through the PIP2/NF-κB/NLRP3 signaling pathway. *Front Immunol*. 2022;13:846384. https://doi.org/10.3389/fimmu.2022.846384.